In situ control of graphene oxide dispersions with a small impedance sensor

Angeliki Eirini DIMOU[1], George MAISTROS[2], Philippe POULIN[3] and
Nikolaos D. ALEXOPOULOS[1*]

[1] Research Unit of Advanced Materials, Department of Financial Engineering, School of Engineering, University of the Aegean, 41 Kountouriotou str., 821 32 Chios, Greece

[2] ADVISE, 17 Gymnasiarchou Madia St., 821 32 Chios, Greece

[3] Centre de Recherche Paul Pascal – CNRS Université de Bordeaux, Avenue Schweitzer, 33600 Pessac, France

Abstract

Carbon-based nanomaterials (CBNs), such as graphene and carbon nanotubes, display advanced physical and chemical properties, which has led to their widespread applications. One of these applications includes the incorporation of CBNs into cementitious materials in the form of aqueous dispersions. The main issue that arises in this context is that currently no established protocol exists as far as characterizing the dispersions. In the present article, an innovative method for quick evaluation and quantification of Graphene Oxide (GO) dispersions is proposed. The proposed method is Electrical Impedance Spectroscopy (EIS) with an impedance sensor. The novelty lies on the exploitation of a small sensor for on-site (field) direct dielectric measurements with the application of alternating current. Five different concentrations of GO dispersions were studied by applying EIS and for various accumulated ultrasonication energies. The low GO concentration leads to high impedance values due to low formed current network. The ultrasonication revealed two opposing mechanisms that are happening simultaneously: it facilitates the flow of the electric current due to the formation of a better dispersed network (break of the agglomerates), nevertheless the surface hydrophilic structure of the GO is damaged with the high accumulated ultrasonication energy. The dielectric measurements were exploited to express an appropriate quantitative "quality index" to facilitate with the dispersion control of the nanostructures. An intermediate concentration of GO is suggested (about 0.15 wt % of the binder materials) to be optimal for the specific engineering application, ultrasonicated at approximately 30 to 65 kJ. The investigated methodology is highly novel and displays a high potential to be applied in-field applications where CBNs must be incorporated in building materials.

Keywords: Electrical Impedance Spectroscopy (EIS); Graphene Oxide (GO); Dispersions; Ultrasonication Energy;

---

[*] Corresponding author: Tel: +30 2271035464. E-mail: nalexop@aegean.gr

1. Introduction

Nanomaterials possess original properties and novel characteristics in comparison to their equivalent bulk materials [1]. One category of nanomaterials is carbon-based nanomaterials (CBNs) and includes among other carbon nanotubes (CNTs), nanodiamonds and Graphene (G). Those materials combine extraordinary physical and chemical properties, *e.g.* electrical conductivity and high mechanical strength [2].

Graphene Oxide (GO) is a derivative of Graphene and contains different oxygen functional groups. These oxygenated groups are the reason for G and GO to have some differences in their mechanical and electrochemical properties, *e.g.* [3]. G and GO have been used so far in many different applications [4], such as lithium-ion batteries, supercapacitors, biosensors, etc. One of the most challenging application of G and its derivatives is their incorporation in construction materials such as cement and concrete. The majority of investigations on this research topic demonstrated that these materials when added in small weight percentages (wt%) in the respective matrices, increase substantially the mechanical, electrical and piezoresistive properties, e.g. by Metaxa [5] and Guo et al. [6].

Possibly the best strategy to incorporate the CBNs in the cement matrix is the prior (appropriate) dispersion of the nanomaterials in the mixing water with cement. This task has been challenging to overcome so far, not only in the case of cement-based composites but also in all CBN applications, since the nanoparticles tend to agglomerate in solutions. This phenomenon leads to the reduction of the specific surface area of the nanoparticles [7], as well as to an inhomogeneous dispersion of the nanoparticles in the cement matrix. Zhao et al. [8] reported that the lack of homogeneity results in the creation of weak zones in the final product. To this end, it is extremely important to break down any-formed agglomerates and to efficiently disperse the nanoparticles in order to form ~~so that~~ a stable system ~~is formed~~. To achieve this goal, different dispersion systems and methods have been investigated in the literature for the CBN dispersion and representative research articles are reported in Table 1~~Table 1~~.

The literature review revealed that the application of ultrasonic energy, is possibly the best means to achieve 'good' CBN dispersions. Several differences were noticed regarding the type of additional agents employed (surfactants, superplasticizers, etc.) to increase the dispersion "quality". There are also several attempts to chemically functionalize the nanomaterials before their dispersion phase. For example, Wang et al. [9] functionalized GO with polyether amine, while Sezer and Koç [10] acid-functionalized CNTs and silver-decorated CNTs to enhance their capability to be efficiently dispersed.

Apart from forming dispersions with the necessary CBN type and concentration, another important issue is their characterization in terms of dispersion degree. The zeta potential (ζ) through Dynamic Light Scattering (DLS) is a widely used method, e.g. in [8], [10] and [11], to characterize an aqueous dispersion. Another method that is frequently exploited to characterize the stability of such dispersions is Ultraviolet-Visible (UV-Vis) Spectroscopy, e.g. [12] and [13]. Vallejo et al. [14] calculated several rheometric parameters, while Konios et al. [15] determined their solubility factors. A literature review with the available methods to characterize the dispersion of nanomaterials in solutions can be found in Table 1Table 1. All these methods can be performed on the same system to get an advanced insight of the dispersion with the combination of all available (conventional and less-conventional) methods for the advanced characterization control. Nevertheless, most of these methods suffer fromare subjected to limitations, like including the need to dilute the suspensions, the use of specific cells with well-defined optical characteristics, the need of large analysis instruments, etc. All these factors are limiting the This widespread and easily implementationis why they cannot be easily implemented for the in-situ characterization of suspensions in various environments and applications.

The present article aims at introducing a light and versatile methodology for the nanomaterials dispersion control with a small sensor by exploiting Electrochemical Impedance Spectroscopy (EIS). By measuring the dielectric properties, process-related conclusions can be madeinvestigated. Dielectric Analysis, also known as impedance spectroscopy, is an already mature technology for the measurement of the dielectric properties, the investigation of the mechanisms and the kinetics of reactions, as well as of properties of porous materials, *e.g.* by Macdonald [16].

As far as the characterization of the dispersions of nanomaterials is concerned, Impedance SpectroscopyEIS has also been applied successfully. For instance, Alfonso et *al*. [17] examined GO solutions in Milli-Q water and Isopropyl Alcohol to find relatively small values of dielectric permittivity in graphene oxide materials in comparison to previous studies. Baltzis et al. [18] applied impedance spectroscopyEIS to study epoxy composites with CNTs and milled carbon and found out that the results indicated an inverse dependence between the magnitude of impedance and the dispersion duration. The reason for this increasing interest on the characterization of systems with this method is the simplicity of the method and the relatively low cost of the measuring technology.

In the present study, a novelty is introduced for the proposed methodology that exploits a small (field) sensor for in-situ direct dielectric measurements with the application of alternating current. It is noted that the classic EIS setup with the parallel electrodes makes the exploitation of the methodology difficult

in on-field applications. Also, EIS has already been applied to study the behaviour of cementitious materials, as described in [19] and [20], but this would not be feasible in field.

The present article focuses on the first step of the production of GO/cement composites, i.e. the development of the aqueous nanoparticle dispersion before being added in the cementitious matrix. The final research target is to produce a composite with electrical and piezoresistive properties, thus permeating the sensing ability. To this end, it will be shown that the proposed method can be used for a quick, efficient, and quantitative evaluation of the CBN dispersions in applications. To achieve this target, five different GO dispersions with varying GO concentration will be produced. Ultrasonication energy with a probe ultrasonicator is applied on all aqueous dispersions and their electrical properties are measured through the application of EIS. The results of the methodology are analysed to characterize the dispersion control and several other analytical techniques like Fourier-Transform Infrared Spectroscopy (FT-IR), Raman Spectroscopy and Optical Microscopy were also used to support the findings of the present investigation.

2. Experimental investigation

The experimental flow diagram can be shortly summarised as follows: firstly, the water and graphene oxide are mixed to form the GO dispersion. Then, ultrasonication energy is applied to the aqueous dispersion, while impedance scans are recorded at different accumulated ultrasonication energy values. Samples at the same ultrasonication values are isolated to be examined with analytical methods, *e.g.* optical microscopy, FT-IR and RAMAN spectroscopy. The results are assessed to fully analyse the aqueous dispersions so that an optimal concentration and amount of ultrasonication energy can be proposed. A schematic representation of the flow diagram of the present article is given in Figure 1.

4

174
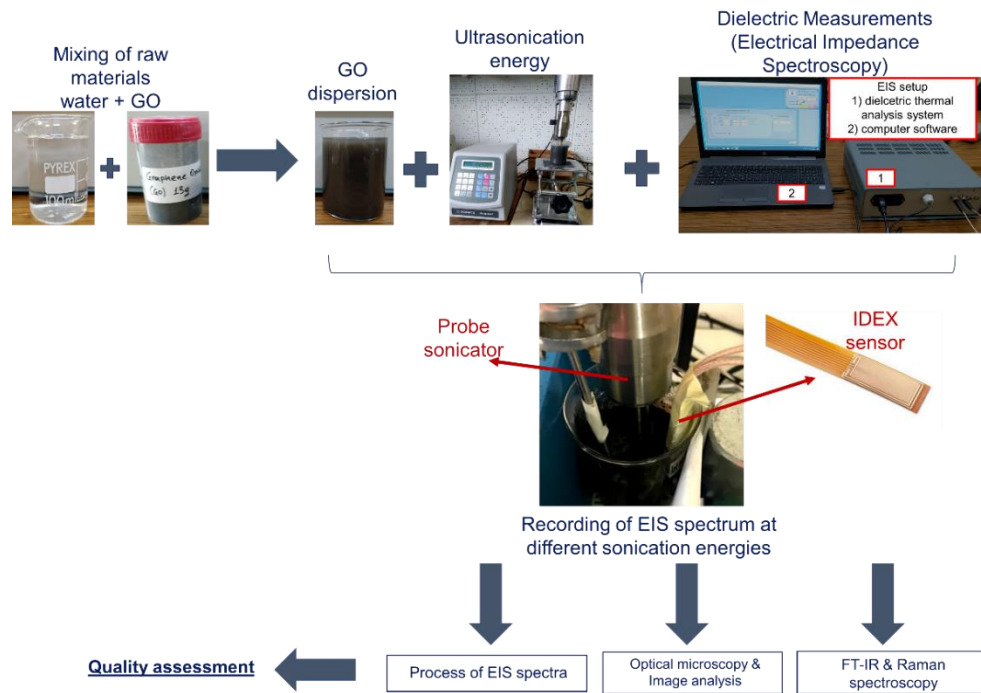
Figure 1. Schematic representation of the experimental procedure.

175

176

177 Table 1: List of dispersion evaluation methods for different dispersion systems of CBNs.

Ref.	Nanomaterial	Dispersion system	Concentration / Content	Dispersion method	Evaluation method
[12]	G	water and superficial active agents (SAAs)	01 wt%, 0.025 wt% and 0.05 wt% (of cement)	1) Stirring of the SAAs and water 2) Ultrasonic disruption in 1 – 6 stages (duration of each stage: 5 min.)	UV-Vis Spectroscopy Sedimentation test
[21]	GNP	water and melamine dispersant	0.2 g GNPs with 1 g dispersant/200 g water/4 g cement.	1) Hand stirring of water and dispersant. 2) High power ultrasonic vibration for 5 min and cooling down in a water bath for another 5 min. (3 times)	Visual rating Image analysis
[22]	Multilayer Graphene Sheets (MLG)	isopropanol	0% to 0.033% by weight of cement	MLG and Isopropanol solutions was directly poured in the matrix. No additives (superplasticizer, water-reducing agents, or surfactants) were employed.	Visual rating Scanning Electron Microscopy (SEM)
[23]	GO	water and superplasticizer (solid power)	0.01 wt%, 0.03 wt%, and 0.05 wt% of cement	1) GO and water were stirred uniformly. 2) The superplasticizer was added and the solution was stirred until complete dissolution 3) The solution was ultrasonicated for 5 min.	Visual rating Atomic force microscopy (AFM)
[10]	Chemically Functionalized Multiwall CNTs	water with and without surfactant	0.1 wt %	Sonication with probe type sonicator for 15 min (3 s pulse, 1 s wait cycles) at constant temperature 23 ° using an ice-cooled bath.	Transition Electron Microscopy (TEM) DLS Thermal conductivity measurements
[14]	Polycarboxylate chemically modified GNPs	propylene glycol and water	0.25, 0.50, 0.75 and 1.0 wt%	Ultrasonication for 200 min in an ultrasound bath	DLS Rheology and viscosity measurements
[11]	GO	solution of chloride salts of Ca^{2+}, K^+ and Na^+	0.035 mg/mL	Sonication for 15 min with a cup-horn sonicate processor	Visual Rating DLS
[15]	GO and reduced GO (rGO)	water and 17 organic solvents	0.5 mg/mL	Sonication in an ultrasound bath cleaner for 1 h and then mildly centrifugation at 500 rpm for 90 min	UV-Vis Spectroscopy Raman Spectroscopy

[17]	GO	Milli-Q water and Isopropyl Alcohol	0.4 – 3 wt %	1) Centrifugation for solvent exchange 2) Sonication with a tip sonicator (30 min) 3) Ultracentrifuge process for 1 h	Electrical Impedance Spectroscopy
[18]	MWCNTs and Carbon Black	two-part low viscosity epoxy resin	0.5 wt % MWCNTs 2 % CB	Shear Mixing - Use of laboratory dissolver apparatus (dispersion under vacuum conditions)	Electrical Impedance Spectroscopy
[24]	CNTs	water-based suspensions with ionic surfactant (added in cement matrix)	0.2 – 0.8 wt % of cement	1) Sonication process 2) Application of vacuum for 45 minutes to remove any residual air bubble	Porosity and pore size distribution measurements (assessment referring to the cement matrix)
[25]	CNTs	Aqueous suspensions with 1) ionic surfactant commonly 2) plasticizer-type dispersant	Surfactant Suspensions 0.5 and 1 wt% CNTs. Dispersant suspensions0.4 - 1.6 wt%	Sonication Process	UV-Vis Spectroscopy
[26]	Single Wall CNTs	Aqueous solutions of sodium dodecylbenzene sulfonate	0.5 wt %	1) Sonication 2) Ultracentrifugation	UV–Vis/NIR spectroscopy Raman spectroscopy Atomic force microscopy

2.1 Materials

Graphene Oxide (GO) was synthesized at the University of Ioannina, Department of Materials Science & Engineering (Prof. D. Gournis and Prof. M. Karakassides), via the following procedure: 10 g graphite (powder) was added to a mixture of 400 mL sulfuric acid (H_2SO_4 95-97 %) and 200 mL nitric acid (HNO_3 65 %) in an ice bath, the mixture was stirred for 45 minutes. Then 100 g powdered $KClO_3$ was slowly added in the mixture in small portions. After 18 h the reaction was terminated by pouring the mixture into deionized water. The product was washed thoroughly until pH of 6.0 was attained. The sample dried at room temperature.

The structural characteristics of Graphite and GO were studied with FT-IR and the results can be seen in Figure 2Figure 2a. Graphite does not absorb infrared light and that explains the absence of clear peaks. On the other hand, GO presents several peaks which come from the vibrations of Oxygen groups, while the carbon double-bond vibrations (C=C) appear at 1630 cm^{-1}. More specifically, the peak at 3440 cm^{-1} corresponds to the extension vibrations of C – OH and the humidity. The peaks at 1720 cm^{-1} and 1059 cm^{-1} come from the carboxyl group vibrations of the bonds C=O and C-O, respectively. The deformation vibrations of hydroxyls of C – OH groups are spotted at 1391 cm^{-1} and finally the peaks at 806 cm^{-1} and 1200 cm^{-1} correspond to the bond vibrations C – O and C – O – C of the epoxy-groups. The results are in accordance with other GO spectra, such as reported in [27] and [28].

The Raman spectrum of GO was measured at the University of Ioannina and is given in the diagram of Figure 2Figure 2b. It where shows all characteristic bands are shown. D Band at 1353 cm^{-1} is attributed

239 to sp^3 hybridization due to imperfections and deformations during Graphite oxidation. 1st order G Band
240 at 1597 cm^{-1} is attributed to sp^2 hybridized carbon atoms of the Graphite net. The ratio (ID/IG) of the D
241 and G bands shows the formation of functional oxygen groups during the oxidation process and was
242 found equal to 0.84.
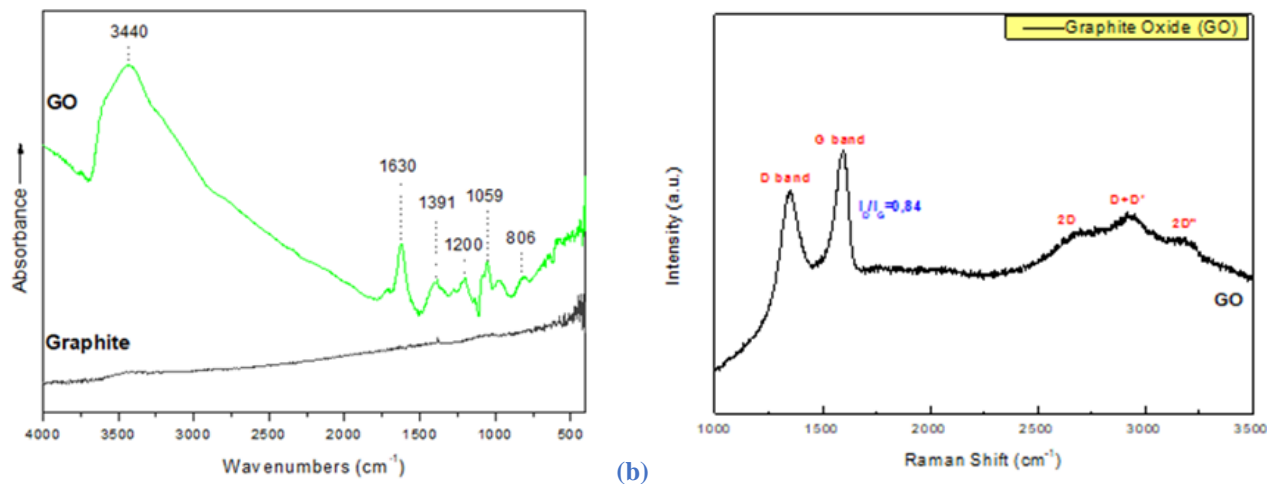
243 **(a)**   **(b)**
244 **Figure 2: (a) FT-IR spectrum of Graphite and GO (b) Raman spectrum of GO.**

245 The dispersion medium in this study was bottled water, more representative of water used in cement
246 applications than Milli-Q water. The water samples were produced by Epirotic Bottling Industry S.A.
247 (VIKOS S.A.), Ioannina, Greece. The pH value of the water sample was 7.3. Shih et al. [29] showed that
248 at low pH values, the carboxyl groups of GO are protonated such that the GO sheets form aggregated
249 due to the lower degree of hydrophilicity. At higher pH, the carboxyl groups are deprotonated. On the
250 other hand, Wu et al. [30] found that at alkaline pH with cation presence GO suspensions destabilize due
251 to cross-linking of GO sheets through interacting with GO surfaces. Taking these facts into account, a
252 product with slightly alkaline pH with low concentration of ions was chosen.

253 **2.2 Experimental methods**

254 Five different GO solutions were prepared and the exact amounts of GO and bottled water are presented
255 in Table 2~~Table 2~~. The GO quantities were selected so as the suspensions could be afterwards used for
256 the preparation of cement-based nanocomposites at concentrations ranging from 0.05 wt% and up to 0.20
257 wt% of the binder, as shown in the last column of Table 2~~Table 2~~. GO and water were weighed and
258 placed in a beaker for the dispersion process and were hand-stirred before the first measurement.

259 **Table 2. Mix proportions of the investigated GO dispersions.**

Solution number (#)	GO (g)	Water (mL)	wt % of binder
GO_0.05	0.07	100	0.05 %
GO_0.10	0.14	100	0.10 %

7

GO_0.15	0.21	100	0.15 %
GO_0.175	0.25	100	0.175 %
GO_0.20	0.28	100	0.20 %

The dispersion process was accomplished by applying ultrasonication energy with a probe type ultrasonicator. The energy generator was the VCX-500 model and the nozzle model was CV-334 model, both produced by the company SONICS & MATERIALS®. A temperature sensor was also used to simultaneously record the temperature values. The process consists of 360 ultrasonication cycles with each cycle containing a 15 s pulse and a 30 s wait. Therefore, the total amount of time needed for each solution is 4.5 h, a time frame that corresponds to about 100 kJ of ultrasonication energy. The ultrasonication experimental setup is shown in Figure 3. The impedance scans were recorded for different accumulated ultrasonication energy values, namely 3 kJ, 12 kJ, 30 kJ, 65 kJ and 100 kJ for 100 mL each of the different investigated GO dispersions.

The effect of ultrasonication energy on the functional groups of GO was also observed for a given concentration (namely 0.15 wt%) through the recording of the FT-IR Spectra with a Brucker – Tensor 27 spectrometer and Raman Spectra. Spectra at different ultrasonication energies were recorded at the same accumulated ultrasonication energy levels, namely at 3 kJ, 12 kJ, 30 kJ, 65 kJ, and 100 kJ. The dispersion evaluation included optical microscopy with a Leica DM-RX microscope at samples ultrasonicated at the respective ultrasonication energy values. The micrographs obtained from the optical microscopy were subjected to image analysis using the ImageJ software [31] to determine the average agglomerates size of agglomerates.
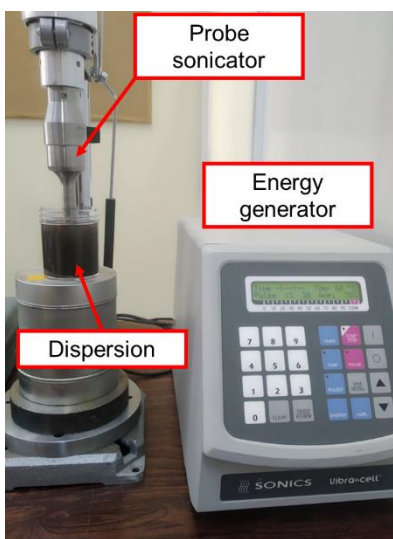

Figure 3. The experimental test set-up with the ultrasonication equipment on the GO dispersion of the present study.

8

EIS was performed during the ultrasonication process using a Dielectric Thermal Analysis System DETA-SCOPE® supplied by ADVISE, Chios, Greece as shown in Figure 4Figure 4. The hardware setup was connected to an interdigital dielectric sensor IDEX®, film-shaped, produced by Netzsch®, Germany. The specific sensor was selected for the present application due to the small geometrical dimensions, approximately 10 mm in width and 30 mm in length. EIS with an IDEX sensor is a high accuracy- and established analysis method already used to investigate various well-known systems, as in [32], [33] and [34].

Additionally, the selected impedance measuring device is light weight, making the whole experimental setup portable and very easy to use in almost all possible applications. The DETA-SCOPE® applies sinusoidal excitation voltage of 10 V amplitude with frequency ranging from 0.1 Hz to 100 kHz. The measurements are recorded by the data acquisition software of the system. The first tests were performed on (plain) bottled water, followed by the five GO dispersions with different GO concentrations. For each dispersion, more than 20 impedance scans were recorded during the whole ultrasonication process and the process was repeated twice for each different concentration of the dispersion. Each dispersion was produced three times (3x) to record the respective spectrum so as to ensure repeatability of the procedure.

Processing and interpretation of the impedance measurements can be accomplished by studying the Equivalent Circuit Model (ECM) [35]. This procedure is usually challenging, because more than one possible solution may fit the experimental data accurately, *e.g.* [36]. The issue of the non-singularity of the fitted model can be overcome if there is a deep understanding of the physiochemical processes and phases included in the system under investigation (*e.g.* double layer capacitance, solution resistance, polarization resistance, or porous electrodes).
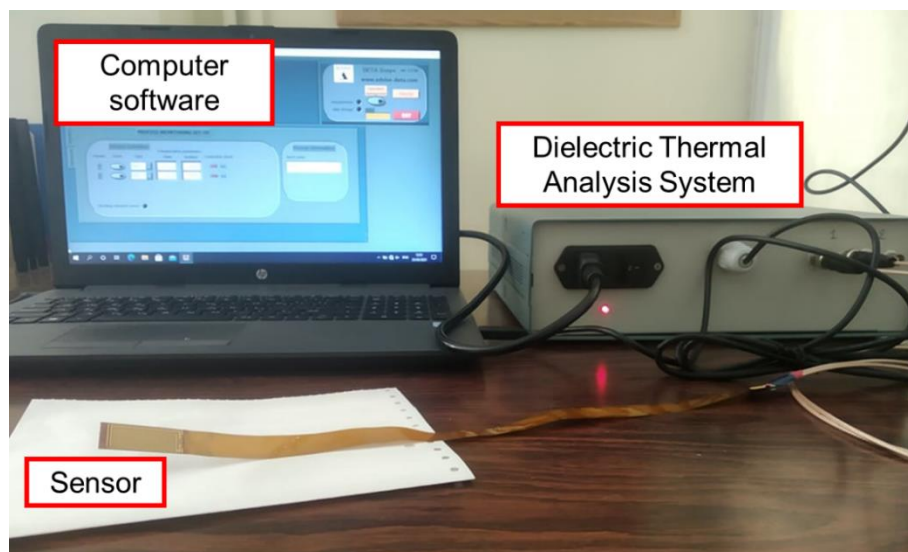

Figure 4. EIS experimental test setup

9

3. Experimental results

3.1 Instrumental analysis methods

The FT-IR spectra were recorded for all the above-mentioned ultrasonication energy values and the results are presented in Figure 5, where the peaks at 1600 cm^{-1} and 1100 cm^{-1} are marked. The goal is to investigate whether the high accumulated ultrasonication energy values can destroy the already formed, specific functional groups. It is already known by Zhang et al. [37] that ultrasonic conditions lead to the exfoliation of graphene oxide [37]. For this reason, the ratio of two standard GO peaks was calculated for the different energies. It is known that the peak at 1600 is related to the sp2 lattice of the Graphene structure, while the 1100 peak refers to C-O- functional group. The ratio of the intensity of the peaks is calculated for all energies (Intensity$_{1600}$ / Intensity$_{1100}$). The calculated ratio increases as the ultrasonication energy value increases, showing that the GO structure is affected by high accumulated ultrasonication energy. All the main peaks continue to exist, but their intensity gradually changes, indicating an affected chemical structure. This implies that a mechanism is evident dealing with the destruction of the functional groups at the surface of the nanostructures, or perhaps The present results could be explained by ato the partial reduction of the GO sheets (exfoliation of graphene oxide) by ultrasonicationsonication. It is also noted that the peak at 2200 - 2500 is attributed to the presence of GO.

The Raman spectra also confirms a change in the GO structure with high accumulated ultrasonication energy values. The characteristic bands are also marked in Figure 5, namely D-band and G-band. The ratio of the intensity of D/G Bands was also calculated and it is acan be considered as a measure of defects in the structure [38]. Likewise, Farah et al. [39] used the same ratio to study the reduction phenomena. As shown in the graph, the ratio of the intensity of those peaks lowers decreases as ultrasonication energy increases, thus showing consistency with the FT-IR results.
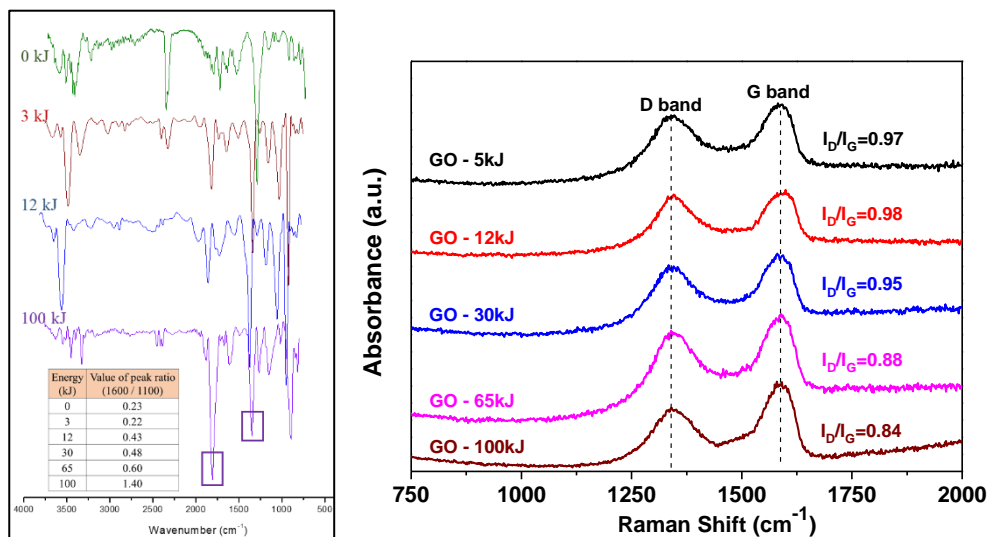
Figure 6Figure 6 displays the images obtained from the optical microscopy analysis and for the different accumulated ultrasonication energy values. As can be seen from the Figure, large agglomerates can be noticed at the non-ultrasonicated samples, since they were not ultrasonicated at all with . Thethe average size of the noticeable agglomerates is being approximately 45 μm. The application of low A small amount of ultrasonication energy level (3 kJ) is enough to break up the largest agglomerates and the nanostructures start to disperse. More specifically, there are two distinct groups of agglomerates can be identified. The first of themgroup contains the larger agglomerates of the order of magnitude of 30 μm in diameter (~ 30 % smaller than the ones with 0 kJ energy) and the second one group contains the lower agglomerates of the order of magnitude of 13 μm in diameter (~ 60 % smaller than the ones with 0 kJ energy). After the application of 12 kJ ultrasonication energy, the nanostructures are even better dispersed and quite few agglomerates were noticed, having with an average diameter of approximate 21 μm.

Further application of ultrasonic ationenergy leads to a better dispersion of the nanoparticles, since the number of the agglomerates is further reduced. For instance, at 30 kJ ultrasonication energy value, the average agglomerate diameter is less than 10 μm. However, at 100 kJ ultrasonication energy value, several agglomerates have started to form again, and the average diameter of the largest ones is approximately 15 - 20 μm, though this time they are uniformly dispersed.

The reason for this re-agglomeration with the high ultrasonication energy level that can be attributed to the alteration of chemical structure of the nanostructures, i.e. the destruction of hydrophilic groups and of the decrease of the lateral size of the GO (often called as exfoliation in the literature). Hydrophobic agglomeration is a phenomenon used to describe the aggregation of hydrophobic particles in aqueous suspension due to the hydrophobic attraction between the particles [40]. Thus, hydrophobic agglomeration takes place, because extensive amounts of ultrasonic energy lead to destruction of hydrophilic groups and a more graphene-like structure (hydrophobic structure).
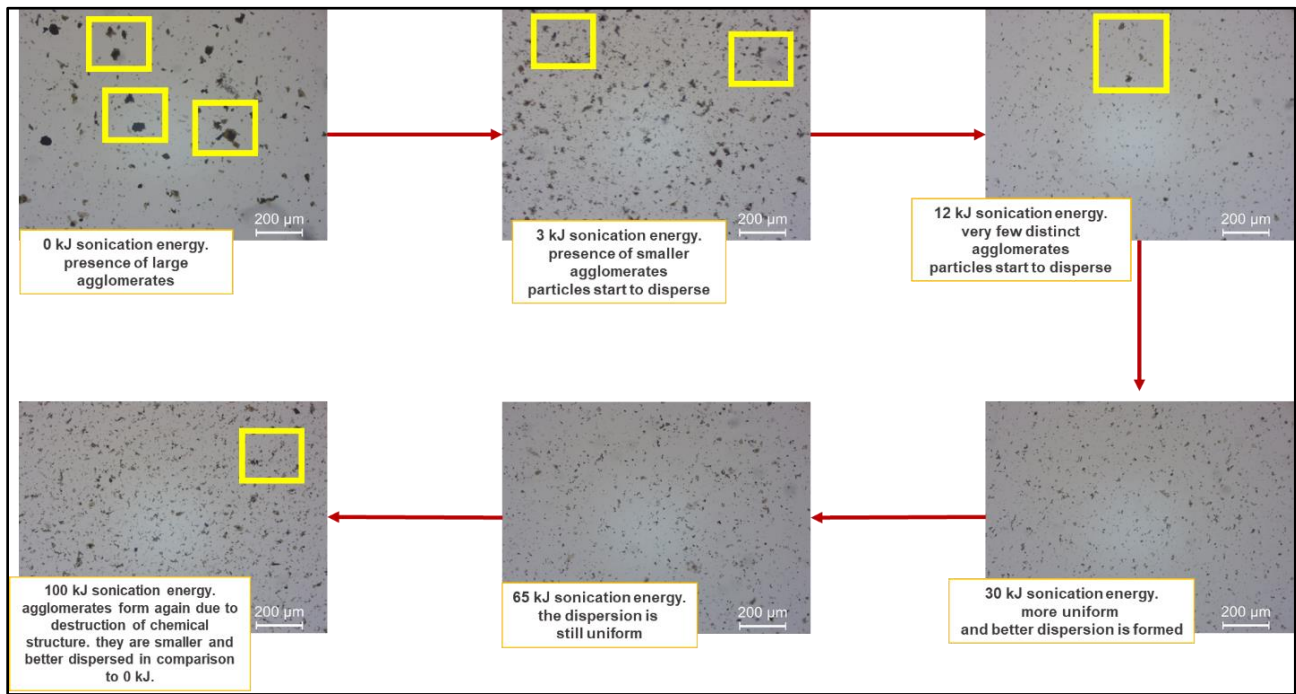
Figure 6: Optical microscopy images for the GO 0.15 wt% dispersion and for the different ultrasonication energy values.

For comparison purposes, Figure 7Figure 7 shows the side view of the beaker with the GO dispersion (100 ml) at 0.15 wt% concentration and for the different investigated ultrasonication energy values. After 12 kJ, the colour of the dispersion seems to be more uniform all over the container. This observation with a naked eye may result to erroneous interpretation, since the optical microscopy results showed completely different results in terms of agglomeration size. To this end, it is recommended that the visual rating is not an appropriate method to evaluate the "quality" of the dispersions or the dispersion control of the nanostructures.
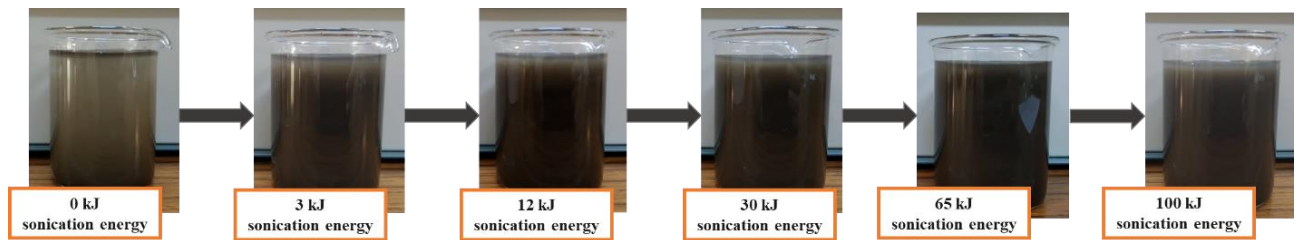
Figure 7: Visual evolution of the side view of the GO 0.15 wt% dispersion for the different investigated ultrasonication energy values.

3.2 Electrical impedance spectroscopy results

The first set of measurements was conducted on bottled water to capture the background impedance of water used in the study and to ensure the repeatability of the procedure. The tests were repeated three times (3x) and repeatability of the dielectric measurements was assured. The Bode impedance plots of

12

453 bottled water in Figure 8Figure 8 present the impedance modulus |Z| and phase angle argZ measurements

454 of the bottled water vs.versus test frequency. As expected, the Bode impedance plot shows that the bottled

455 water is not affected by the ultrasonication energy level and the impedance vector is characteristic of

456 water.
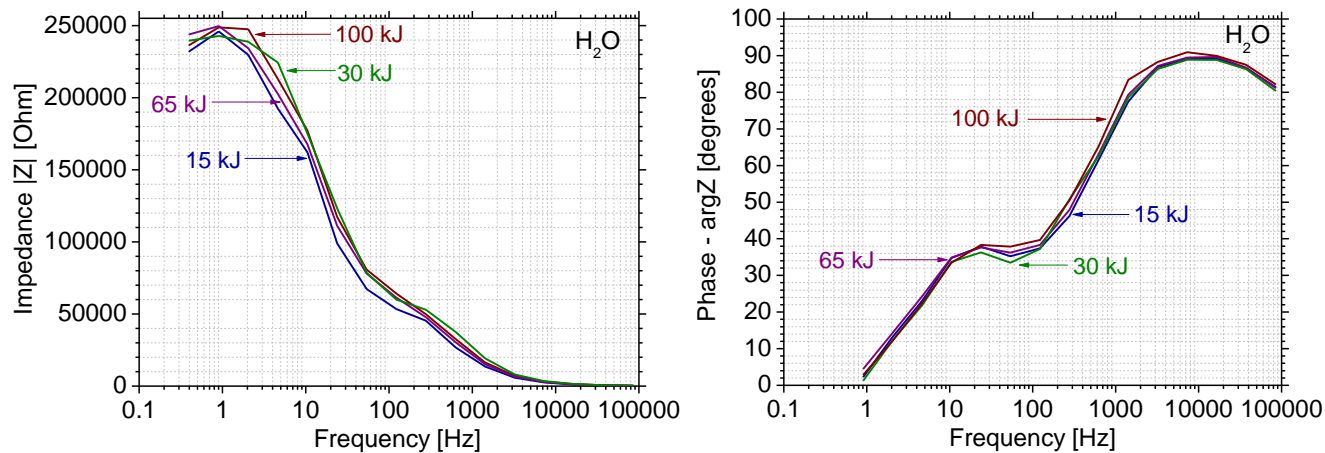
457

458 **Figure 8: Measurements of impedance modulus (left) and phase angle (right) versus test frequency for the bottled**

459 **water (solvent).**

460 The Bode impedance plots in Figures 9a to 9e refer to the five (5) investigated GO concentrations and

461 present the impedance vector against test frequency for different accumulated ultrasonication energy

462 values. The GO_0.05 dispersion exhibits the highest impedance modulus values. There is a general

463 tendency for increasing impedance modulus at low frequencies when the ultrasonication energy increases

464 with the exception of the highest GO concentration. The dominance of ionic conductivity is evident in

465 the GO dispersions at frequencies below 100 Hz considering the interdigital structure of the sensors and

466 the fringing electric field created above the sensor surface. The above-mentioned tendency could be a

467 result of partial reduction of GO with ultrasonication as there will be less ions after reduction. As the

468 concentration of GO in the aqueous dispersions increases, the overall magnitude of the impedance vector

469 decreases indicating higher concentration of charged species, such as ions, in the electric field.

470 Qualitative and quantitative analysis of the spectra will be made discussed in the following section.

13
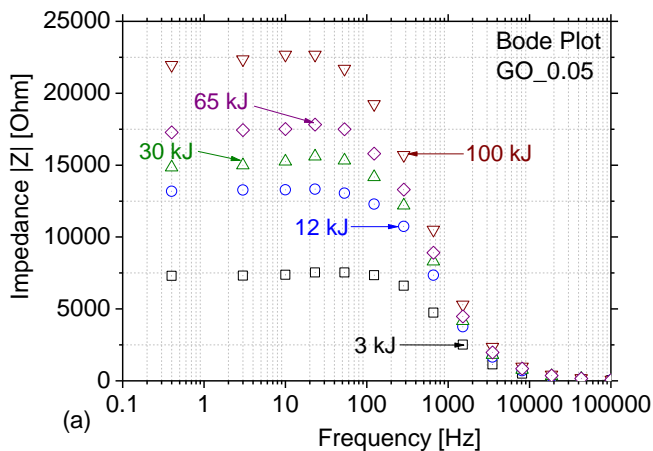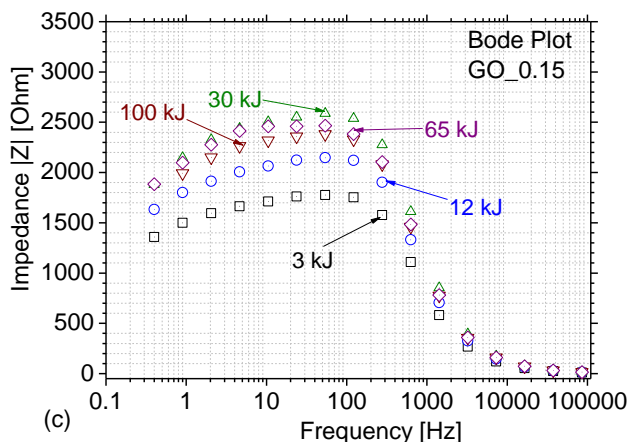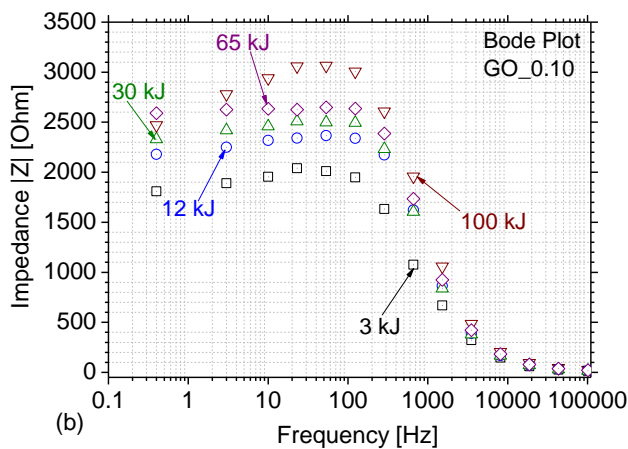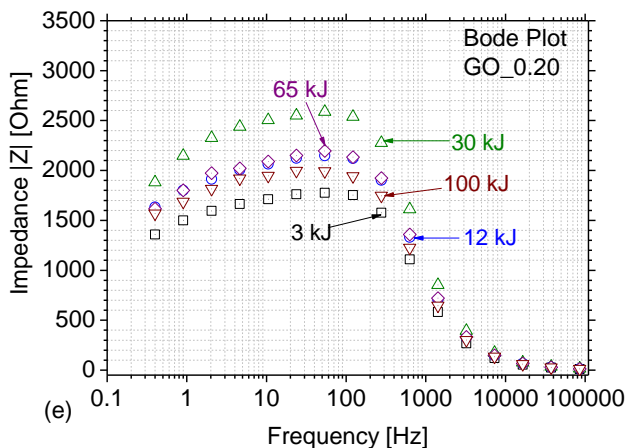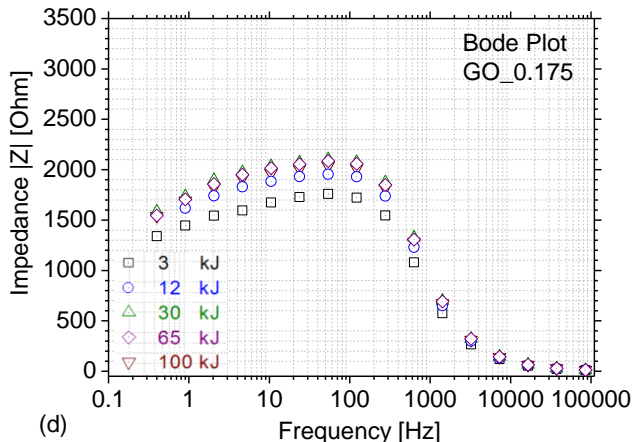
Figure 9: Bode plots of the five different investigated GO dispersions (GO concentration from 0.05 wt% and up to 0.20 wt%) at different ultrasonication energy levels.

As the ultrasonication energy increases, it is expected that the dispersion becomes more uniform with lower size of agglomerates as well as that GO reduction is promoted. Both of these effects lead to increasing impedance levels in the GO dispersion. By the application of ultrasonication energy; the form of cavitation micro-bubbles and their collapse because of the energy excess leads to the creation of micro-jets and shockwaves, thus facilitating de-bundling to achieve better dispersion of nanoparticles [41].

4. Discussion of the results

4.1 Analysis of the impedance values

The output results of the ~~electrical impedance~~EIS experiments are the modulus of the electrical impedance |Z| and the phase angle of the impedance ~~θ~~, from which the real and imaginary part of the resistance can be calculated. Figure 10 presents the real and imaginary impedance parts for all GO dispersions and the different, pre-defined accumulated ultrasonication energy levels. At the concentrations of 0.05 wt.% and 0.10 wt.%, the real part of the impedance at low frequencies increases as the ultrasonication energy level increases. This effect is less pronounced as the GO concentration in the dispersions increases. At all GO concentrations higher than 0.05 wt %, two distinct relaxation processes are observed in the imaginary impedance plots on either side of the minimum value at the frequency of 25 Hz.
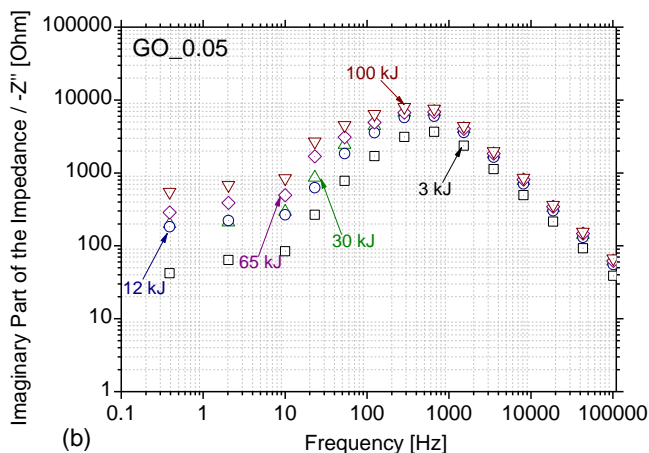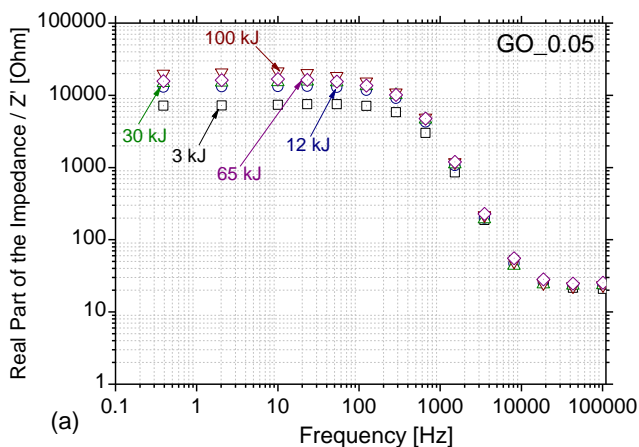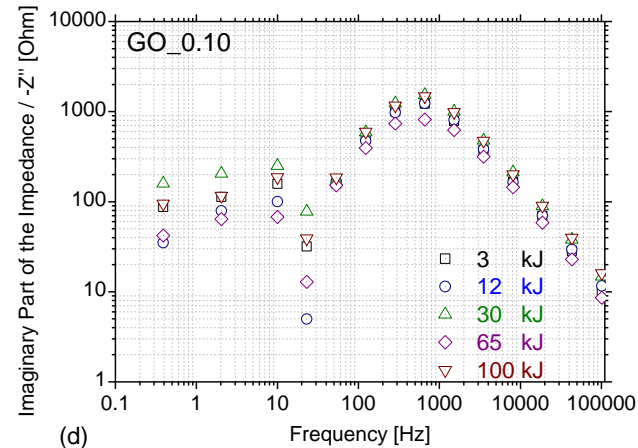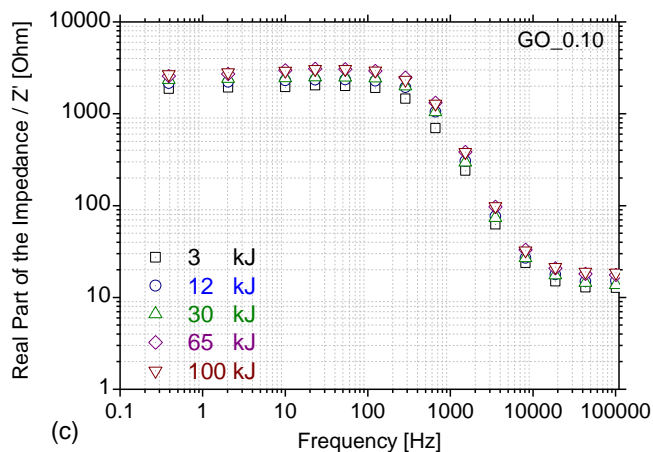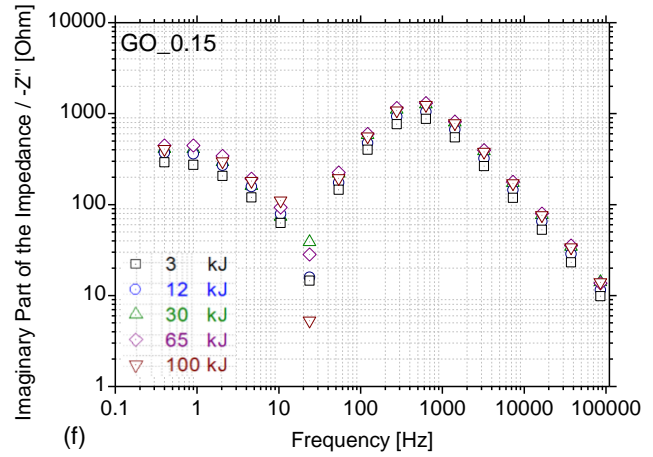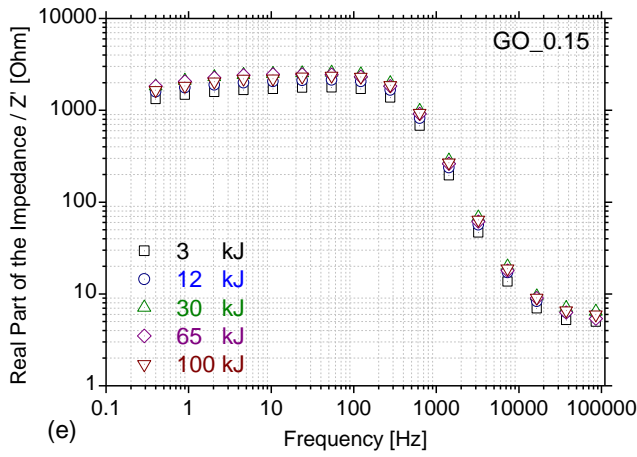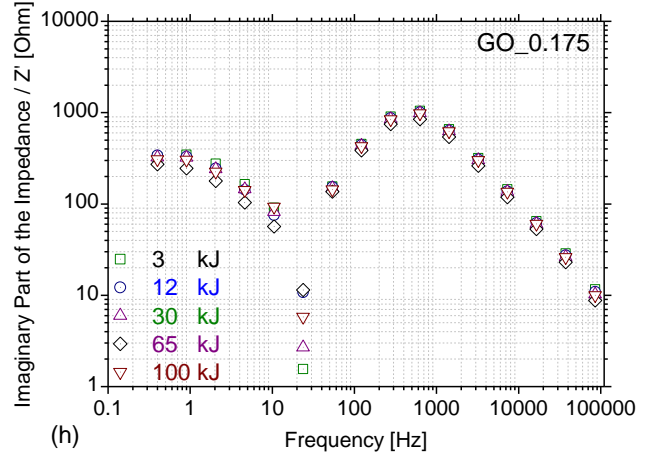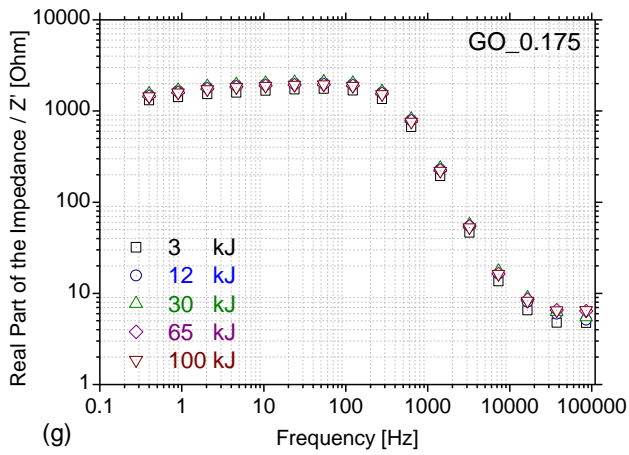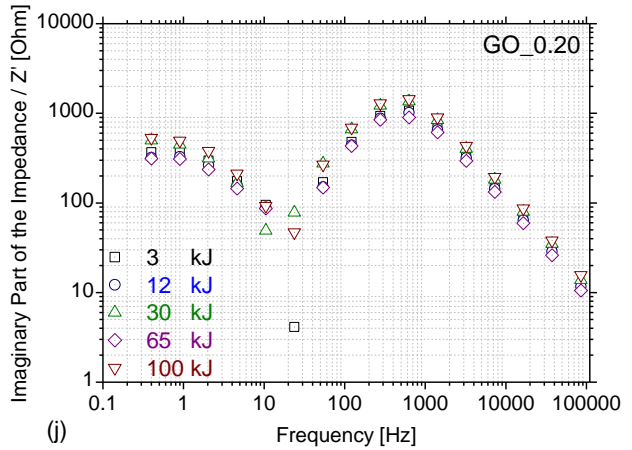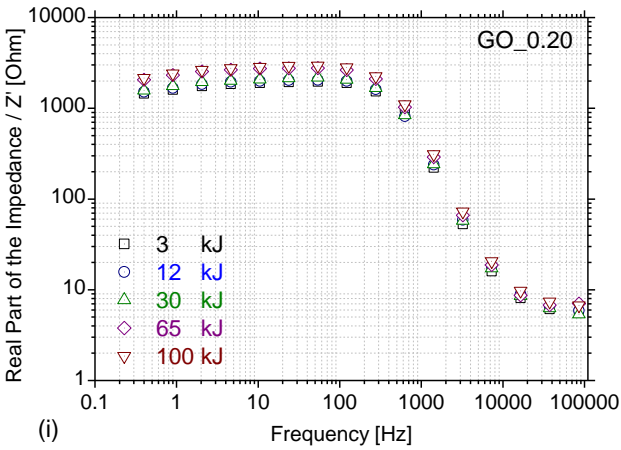
Figure 10. Real and imaginary parts of the impedance for the investigated GO dispersions (GO concentration from 0.05 wt% and up to 0.20 wt%) and for the different ultrasonication energy levels.

4.2 Equivalent circuit modelling

The proposed equivalent circuit modelling (ECM) is an evolution of the classical Randle-cell model [42] that contains elements corresponding to the different processes present in our system, i.e. the interface between the dispersion, ~~and~~ the Kapton film of the sensor and the active phase of nanoparticles dispersion. As shown in Figure 11, the ECM consists of two branches according to the previous

16

description with four elements. The capacitor C_1 and the resistor R_1 are the double layer capacitance and the charge transfer resistor, respectively and they refer to the electrical double layer at the interface of the dispersion and the film. In series with this branch we find the components of the water / GO nanostructures phase in terms of a parallel connection of the constant phase element (*CPE*), which is symbolized with Q, and the resistor R_2.
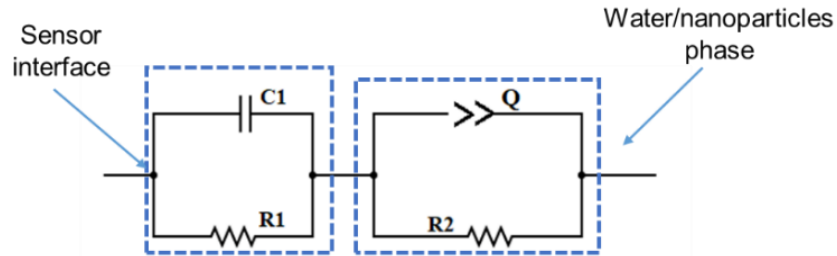
Figure 11: Proposed equivalent circuit model for the aqueous GO dispersions.

**Table 34: Characteristics of the elements used for the proposed equivalent circuit model.**

Element	Impedance (Z)	Units
R_1, R_2	R	Ohm
Q (or *CPE*)	$1/[Q_0(j\omega)^n]$	$F \cdot s^{n-1}$
C	$1/(j\omega C)$	F

CPE is a non-intuitive circuit element that is used to describe responses of real-world systems [43] and will be used in the present investigation to address ~~in our system the reasons for its appearances are~~ inhomogeneity and non-uniform current distribution. Q_0 corresponds to the admittance of the ideal capacitance and n is a constant with a range of 0 to 1, with $n = 1$ referring to a pure capacitor and $n = 0$ referring to a pure resistor, e.g. [43]. Likewise, Han et al. [44] introduced the constant phase elements to describe stacked graphene oxide in solid humidity sensors. As reported in ~~that study~~this research article and also noted in the present ~~research~~investigation, the frequency behaviour of GO is too complicated to be presented using simple RC circuits. Hence, the introduction of *CPE* was deemed necessary as a circuit component, commonly used to express an imperfect capacitor in a circuit of distributed resistors and capacitors. The reason for this non-uniform current distribution lies firstly on the van der Waals attractions among nanoparticles and the double-layer electrostatic repulsions, e.g. [30] and [45]. Also, the presence of metal and non-metal ions can cause a destabilisation of the GO mixtures, playing a critical role in the dispersion [46].

Figure 12 shows the equivalent circuit model (ECM) predictions versus the experimental results for a given ultrasonication energy, namely 65 kJ and for three different GO dispersions. It can be seen that the

17

553 proposed ECM fits well to the experimental results. The parameter values derived from the ECM analysis

554 are given in Table 5, again for the 65 kJ ultrasonication energy and for all investigated concentrations.


555
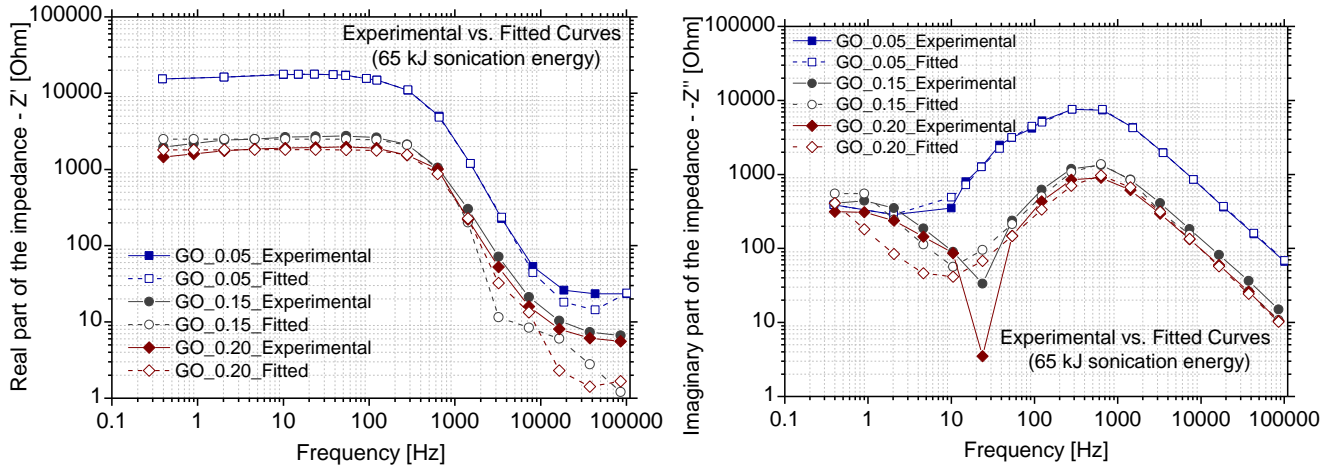
Figure 12: Calculated results for the proposed equivalent circuit model at 65 kJ ultrasonication energy and for three different GO concentrations.

558 **Table 45: Values of the circuit elements of the model shown in Figure 11 for all different GO concentrations at 65 kJ**

559 **ultrasonication energy value and the respective relative standard deviation.**

| Element	GO_0.05	GO_0.10	GO_0.15	GO_0.175	GO_0.20
R_1 (Ohm)	$1.6 \cdot 10^4$ (± 1.3 %)	$2.1 \cdot 10^3$ (± 7.9 %)	$1.8 \cdot 10^3$ (± 3.7 %)	$1.8 \cdot 10^3$ (± 6.8 %)	$2.2 \cdot 10^3$ (± 7.7 %)
C_1 (F)	$2.2 \cdot 10^{-8}$ (± 1.2 %)	$4.4 \cdot 10^{-4}$ (± 1.5 %)	$7.5 \cdot 10^{-4}$ (± 27.4 %)	$6.4 \cdot 10^{-4}$ (± 21.8 %)	$9.8 \cdot 10^{-4}$ (± 28.5 %)
R_2 (Ohm)	$1.6 \cdot 10^3$ (± 14.3 %)	$2.5 \cdot 10^3$ (± 1.0 %)	$2.4 \cdot 10^3$ (± 2.2 %)	$1.9 \cdot 10^3$ (± 2.3 %)	$1.8 \cdot 10^3$ (± 2.5 %)
Q ($F \cdot s^{n-1}$)	$2.2 \cdot 10^{-7}$ (± 27.2 %)	$2.2 \cdot 10^{-7}$ (± 13.7 %)	$7.1 \cdot 10^{-8}$ (± 32.1 %)	$7.8 \cdot 10^{-8}$ (± 35.5 %)	$9.9 \cdot 10^{-8}$ (± 39.4 %)
n (-)	0.98 (± 5.2 %)	0.98 (± 1.6 %)	0.96 (± 4.1 %)	0.96 (± 5.1 %)	0.94 (± 4.5 %)

560

561 Although there is an overall good fit of the experimental data, the proposed circuit fails to model the

562 relaxation phenomenon with high accuracy and more specifically the local minimum in the imaginary

563 impedance spectra. For that reason, a revised ECM has been proposed to model the response of the

564 dispersions for GO concentrations higher than 0.10 wt.%, which is presented in Figure 13Figure 13. In

565 an attempt to improve the representation of the electrode polarisation phenomena at the sensor surface at

566 lower frequencies and its separation to the relaxation phenomena at the bulk of the dispersion, the $C - R_1$

567 branch of the first ECM is replaced by a capacitor in series with a Q-R element. The addition of an extra

568 Q-R element in series to the first proposed circuit will be more suitable for the high concentrations of the

569 GO dispersions, but it will be not so appropriate for the dilute solutions. Figure 14 demonstrates the

570 fitting results of GO_0.15 dispersion at different ultrasonication energy values, while the respective

571 values of each element can be seen in Table 6. The comparison of the fit of ECMs to the experimental

572 data shows that the values of the parameters in both Q-R elements change slightly within the range of the

573 standard deviation of their values. Because the n values of the CPEs is close to 1, the Q value is

18

representative a pure capacitor, and the fact that the Q value remains nearly unchanged makes sense physically as the permittivity of the solution is expected to remain unchanged considering the low concentration of GO in the dispersion. Furthermore, the observed slight drop in R_2 is expected as the GO concentration increases. Therefore, to accurately model the dispersion, the sensor interphase is better described by the revised ECM.
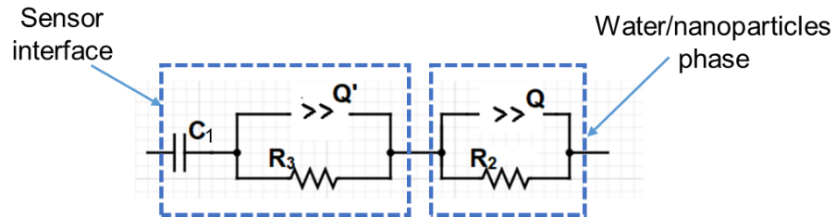
Figure 13: Updated ECM for the investigated GO dispersions with GO concentrations higher than 0.10 wt.%.
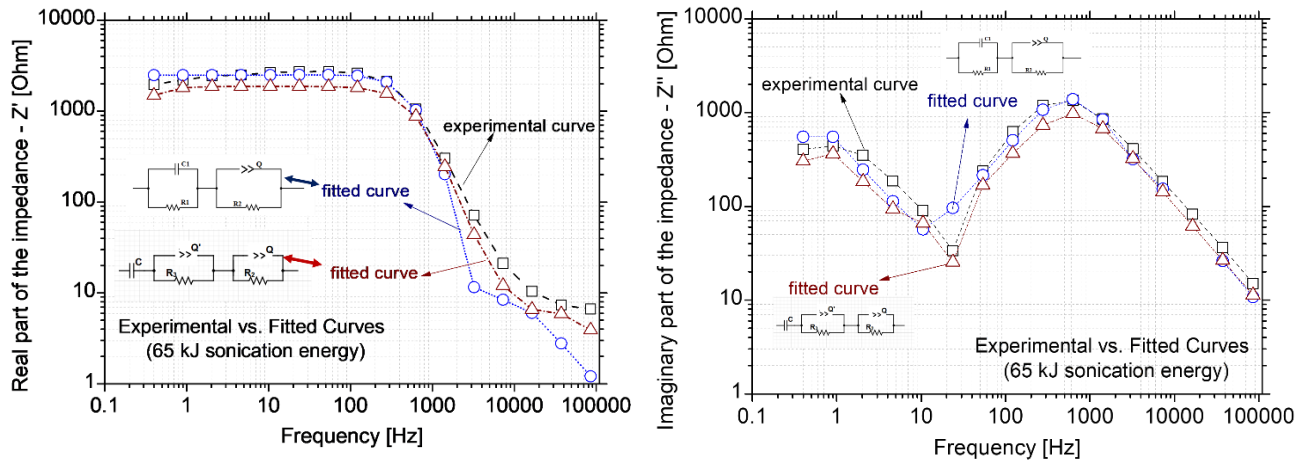
Figure 14: Comparison of the predictions the two proposed circuit models at higher GO concentrations for the (a) real and (b) imaginary parts of the impendance.

Table 56: Values and the respective relative std. deviation of the proposed circuit elements at the updated ECM at 65 kJ ultrasonication energy value.

Element	GO_0.15	GO_0.175	GO_0.20
C_1 (F)	$2.9 \cdot 10^{-4}$ (± 6.3 %)	$3.4 \cdot 10^{-4}$ (± 34.1 %)	$4.2 \cdot 10^{-4}$ (± 45.3 %)
R_3 (Ohm)	$2.4 \cdot 10^3$ (± 7.7 %)	$2.1 \cdot 10^3$ (± 7.1 %)	$1.8 \cdot 10^3$ (± 9.6 %)
Q' (F)	$1.2 \cdot 10^{-4}$ (± 3.4 %)	$1.5 \cdot 10^{-4}$ (± 3.2 %)	$1.7 \cdot 10^{-4}$ (± 4.1 %)
n' (-)	1.03 (± 46.3 %)	1.02 (± 44.1 %)	1.03 (± 57.0 %)
R_2 (Ohm)	$2.3 \cdot 10^3$ (± 1.4 %)	$2.0 \cdot 10^3$ (± 1.4 %)	$1.8 \cdot 10^3$ (± 1.6 %)
Q (F·s^{n-1})	$7.6 \cdot 10^{-8}$ (± 22.1 %)	$9.5 \cdot 10^{-8}$ (± 21.4 %)	$1.2 \cdot 10^{-7}$ (± 25.7 %)
n (-)	0.96 (± 4.1 %)	0.98 (± 2.4 %)	0.97 (± 2.9 %)

The values of R_2 and Q are given in Figure 15 as a function of ultrasonication energy and for different GO concentrations. As far as the dependence of the ultrasonication energy on the ECM parameter values is concerned, the fit has revealed small changes on the Q-R element of the water – nanoparticles phase.

19

590 As the *n* value remained close to 1, *Q* is representative of pure capacitor and its value did not change

591 with the ultrasonication energy for each GO concentration. ~~During sonication~~ T~~t~~here are two effects with

592 opposing expected effects on the impedance during ultrasonication: the breaking of GO agglomerates

593 towards a finer distribution which decreases the distance between the nanoparticles in the dispersion,

594 thus decreasing impedance levels. The second effect is the ~~and the~~ damage in the hydrophilic nature of

595 the nanostructure with simultaneous ~~reduction~~ decrease of the lateral size of GO, which increases the

596 impedance level. These effects cannot be discerned in the impedance spectra and the resulting parameters

597 of the ECMs. To this end, a sort of a kind of "optimal" ultrasonication energy must be considered to

598 introduce the appropriate energy to break the large GO agglomerates and not to completely destroy the

599 surface structure of the GO nanoparticles.
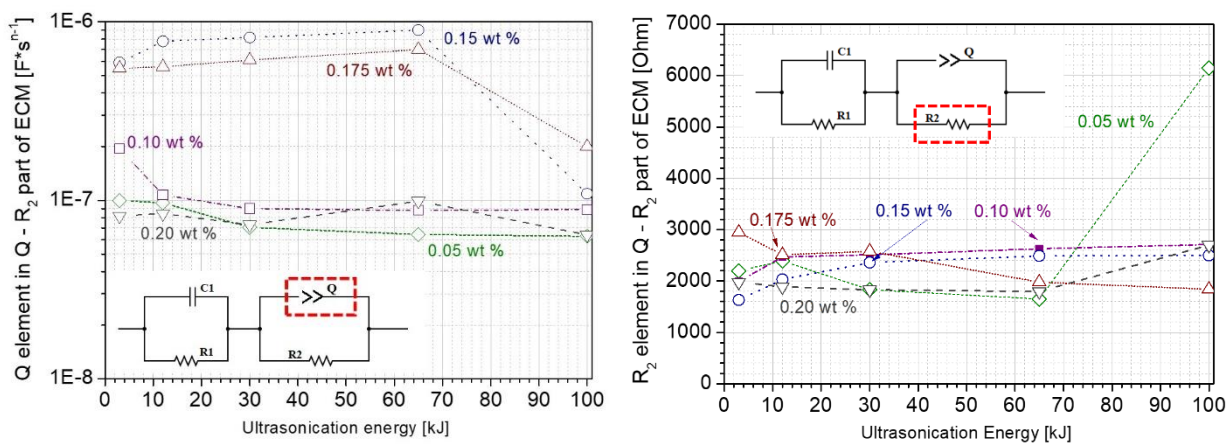
Figure 15: Values of elements *Q* (left) and *R₂* (right) of the proposed electrical circuit models.

## 4.3 Introduction of a quality index in aqueous dispersions

604 To facilitate the evaluation of the dispersion (dispersion control), a relevant quality index (QI) will be

605 proposed. To this end, the proposed quality index can facilitate the dispersing stage of the nanostructures

606 that, in latter stage, the appropriate dispersion can be mixed with the binder material and thus can be

607 applied for the appropriate intervention.

608 Having examined the dispersion in terms of dielectric properties and having performed the appropriate

609 instrumental analysis methods, the quality index that is proposed is the real part of the impedance [Z´] at

610 a high frequency, higher than 10 kHz. The choice of the real part of the impedance was based on the fact

611 that a decrease in Z´ is an indication of simple electrolyte in the solution, *e.g.* [17]. The suggestion of a

612 high frequency value was selected in order to avoid polarisation and/or the relaxation phenomena that

613 appear in lower frequencies in many physical and chemical systems, *e.g.* [47], [48]. In present study, Z´

614 is taken at 20 kHz, as described in the following eqn. (1):

$$QI = Z' = |Z| \cdot \cos(\arg|Z|) \; at \; high \; frequency \; (higher \; than \; 20 \; kHz) \qquad (1)$$

As shown in Figure 16, Z′ decreases as concentration increases, but for constant ultrasonication energy level. As far as the ultrasonication energy is concerned, Z′ presents a minimum at an intermediate ultrasonication energy and for all investigated GO concentrations. This is logical, since the structure has been affected due to partial destruction of functional groups, as shown by Raman and FT-IR analyses in the previous sections. Taking Figure 16 into consideration, which contains all the previous analysis, for any concentration higher than GO_0.10 the Z′ value is distinctively small, thus resembling a good electrolyte. Regarding ultrasonication energy, all GO concentrations display a local minimum at medium values of ultrasonication energy of 30 kJ or 65 kJ. Therefore, an optimal combination of 0.15 wt% of the binder ultrasonicated at about approximate 60 kJ is proposed, since it would require a smaller GO concentration that would lead to less material used in real engineering applicationsconsumption. However, any range from 0.15 wt % up to 0.20 wt % of the binder ultrasonicated at an intermediate energy level could be accepted.

To this end, the involvement of a quality index for the dispersion control of relevant nanostructures is very tempting and would facilitate the quantitative selection by means of the appropriate concentration, type and ultrasonication energy of the nanostructures. To the best of the authors' knowledge, such a quantitative index is not proposed in the literature so far for the dispersion control of any kind of nanostructures.
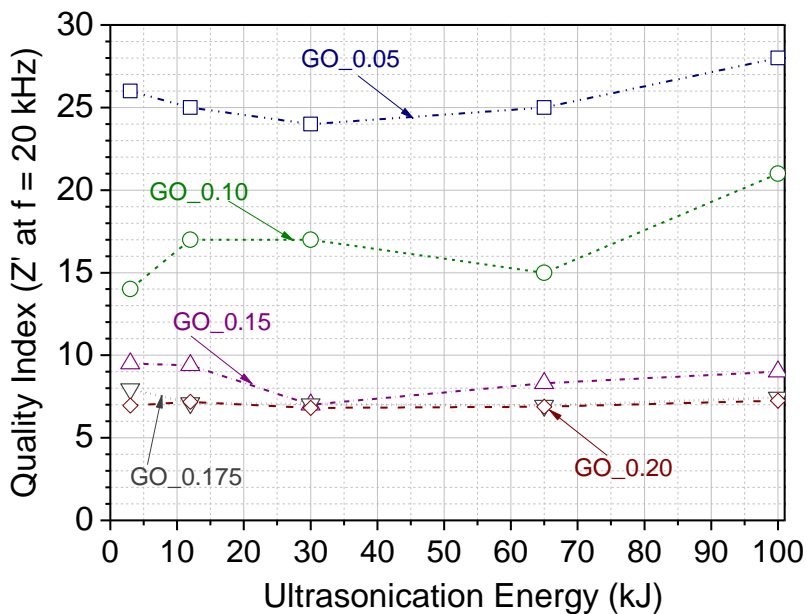
Figure 16: Variance of the proposed quality index as a function of ultrasonication energy and for the different investigated GO dispersions.

5. Conclusions

The conclusions of the present investigation can be summarised as follows:

- A novel method to study aqueous carbon nanostructure (Graphene Oxide – GO in the present investigation) dispersions is investigated, based on alternative current electrochemical impedance spectroscopy. The novelty also lies on the application of a very small sensor that can be used on field applications, where the application of instrumental analysis methods is not possible.

- The application of ultrasonication energy leads to two competing mechanisms. At the beginning the ultrasonic energy contributes to the formation of conductive networks as it effectively breaks the agglomerates. This was confirmed by dielectric measurements through the change in impedance values as well as by analytical investigations. Nevertheless, at high energy level the ultrasonication destroys the surface groups of the nanostructures and the GO-particles, decreases their lateral size and at high energy level tend to re-agglomerate.

- The GO-dispersions were modelled with the use of several equivalent circuit models. A constant phase element was found to better describe the inhomogeneities of the dispersion.

- A quality index was proposed for a quick, quantified evaluation of the dispersion degree. It is proposed this index to be equal to the real part of the impedance at a high frequency, as it is easy to be calculated and a low value in Z′ is an indication of simple electrolyte in the solution. Additionally, there are no polarisation phenomena in such high frequencies.

- Based on the investigation on the specific application (i.e. nanostructures in aqueous solution for civil engineering applications), the optimal combination of concentration and ultrasonication energy is 0.15 wt% of the binder with ultrasonication energy values of approximate 30 to 65 kJ.

Conflict of Interest

The authors declare that there are no known conflicts of interest associated with this publication.

Author Contributions

Conceptualization: N.D.A. and G.M.; methodology: A.E.D. and G.M.; experimental work: A.E.D.; validation: N.D.A., G.M., P.P. and A.E.D.; writing-original draft preparation: A.E.D.; writing – review and editing: N.D.A., G.M. and P.P.; All authors read and approved the manuscript.

References

[1] A. Alagarasi, "Chapter: 1," in *Introduction to Nanomaterials*, 2011, p. 76.

[2] C. Cha, S. Shin, N. Annabi, M. Dokmeci and A. Khademhosseini, "Carbon-Based Nanomaterials: Multi-Functional Materials for Biomedical Engineering," *ACS Nano,* vol. 7, no. 4, p. 2891–2897, 2013.

[3] S. Park, K. Lee, G. Bozoklu, W. Cai, S. Nguyen and R. Ruoff, "Graphene Oxide Papers Modified by Divalent Ions—Enhancing Mechanical Properties via Chemical Cross-Linking," *ACS Nano,* vol. 2, no. 3, pp. 572-578, 2008.

[4] A. Lawal, "Graphene-based nano composites and their applications. A review," *Biosensors and Bioelectronics,* vol. 141, pp. 11384-, 2019.

[5] Z. Metaxa, "Exfoliated graphene nanoplatelet cement-based nanocomposites as piezoresistive sensors: influence of nanoreinforcement lateral size on monitoring capability," *Ciência & Tecnologia dos Materiais,* vol. 28, no. 1, pp. 73-79, 2016.

[6] R. Guo, Y. Suo, H. Xia, Y. Yang, Q. Man and F. Yan, "Study of Piezoresistive Behavior of Smart Cement Filled with Graphene Oxide," *nanomaterials,* vol. 11, p. 206, 2021.

[7] Y. Zare, K. Y. Rhee and D. Hui, "Influences of nanoparticles aggregation/agglomeration on the interfacial/interphase and tensile properties of nanocomposites," *Composites Part B,* vol. 122, pp. 41-46, 2017.

[8] L. Zhao, X. Guo, Y. Liu, C. Ge, Z. Chen and L. Guo, "Investigation of dispersion behavior of GO modified by different water," *Carbon,* vol. 128, pp. 255-269, 2018.

[9] M. Wang, H. Yao, R. Wang and S. Zheng, "Chemically functionalized graphene oxide as the additive for cement–matrix composite with enhanced fluidity and toughness," *Construction and Building Materials,* vol. 150, pp. 150-156, 2017.

[10] N. Sezer and M. Koç, "Stabilization of the aqueous dispersion of carbon nanotubes using different approaches," *Thermal Science and Engineering Progress,* vol. 8, pp. 411-417, 2018.

[11] A. Sabziparvar, E. Hosseini, V. Chiniforush and A. Korayem, "Barriers to achieving highly dispersed graphene oxide in cementitious composites: An experimental and computational study," *Construction and Building Materials,* vol. 199, pp. 269-278, 2019.

[12] J. Liu, J. Fu, Y. Yang and C. Gu, "Study on dispersion, mechanical and microstructure properties of cement paste incorporating graphene sheets," *Construction and Building Materials,* vol. 199, pp. 1-11, 2019.

[13] D. Li, M. B. Muller, S. Gilje, R. B. Kaner and G. G. Wallace, "Processable aqueous dispersions of graphene nanosheets," *Nature Nanotechnology,* vol. 3, no. 2, pp. 101-105, 2008.

[14] J. P. Vallejo, G. Żyła, J. Fernández-Seara and L. Lugo, "Rheological behaviour of functionalized graphene nanoplatelet nanofluids based on water and propylene glycol:water mixtures," *International Communications in Heat and Mass Transfer,* vol. 99, pp. 43-53, 2018.

[15] D. Konios, M. M. Stlylianakis, E. Stratakis and E. Kymakis, "Dispersion behaviour of graphene oxide and reduced graphene oxide," *Journal of Colloid and Interface Science,* vol. 430, pp. 108-112, 2014.

[16] D. D. Macdonald, "Reflections on the history of electrochemical impedance spectroscopy," *Electrochimica Acta,* vol. 51, pp. 1376-1388, 2006.

[17] M. Alfonso, J. Yuan, F. Tardani, W. Neri, A. Colin and P. Poulin, "Absence of giant dielectric permittivity in graphene oxide materials," *Journal of Physics Materials,* vol. 2, p. 045002, 2019.

[18] D. Baltzis, D. Bekas, G. Tzachristas, A. Parlamas, M. Karabela, N. Zafeiropoulos and A. Paipetis, "Multi-scaled carbon reinforcements in ternary epoxy composite materials: Dispersion and electrical impedance study," *Composites Science and Technology,* vol. 153, pp. 7-17, 2017.

[19] F. He, R. Wang, C. Shi, R. Zhang, C. Chen, L. Lin and X. An, "Differential analysis of AC impedance spectroscopy of cement-based materials considering CPE behavior," *Construction and Building Materials,* vol. 143, pp. 179-188, 2017.

[20] H. Sun, Z. Ren, S. A. Memon, D. Zhao, X. Zhang and D. Li, "Investigating drying behavior of cement mortar through electrochemical impedance spectroscopy analysis," *Construction and Building Materials,* vol. 135, pp. 361-368, 2017.

[21] J. Tao, X. Wang, Z. Wang and Q. Zeng, "Graphene nanoplatelets as an effective additive to tune the microstructures and piezoresistive properties of cement-based composites," *Construction and Building Materials,* vol. 209, pp. 665-678, 2019.

[22] R. e Silva, P. de Castro Guetti, M. da Luz, F. Rouxinol and R. Gelamo, "Enhanced properties of cement mortars with multilayer graphene nanoparticles," *Construction and Building Materials,* vol. 149, pp. 378-385, 2017.

[23] H. Peng, Y. Ge, C. Cai, Y. Zhang and Z. Liu, "Mechanical properties and microstructure of graphene oxide cement-based composites," *Construction and Building Materials,* vol. 194, pp. 102-109, 2019.

[24] P. Alafogianni, K. Dassios, C. Tsakiroglou, T. Matikas and N. Barkoula, "Effect of CNT addition and dispersive agents on the transport properties and microstructure of cement mortars," *Construction and Building Materials,* vol. 197, pp. 251-261, 2019.

[25] P. Alafogianni , K. Dassios, S. Farmaki, S. Antiohos, T. Matikas and N.-M. Barkoula, "On the efficiency of UV–vis spectroscopy in assessing the dispersion quality in sonicated aqueous suspensions of carbon nanotubes," *Colloids and Surfaces A: Physicochemical and Engineering Aspects,* vol. 495, pp. 118-124, 2016.

[26] A. Blanch, C. E. Lenehan and J. S. Quinton, "Parametric analysis of sonication and centrifugation variables for dispersion of single walled carbon nanotubes in aqueous solutions of sodium dodecylbenzene sulfonate," *Carbon,* vol. 49, pp. 5213-5228, 2011.

[27] C. Valencia, C. H. Valencia, F. Zulaga, M. E. Valencia and J. H. Mina, "Synthesis and Application of Scaffolds of Chitosan-Graphene Oxide by the Freeze-Drying Method for Tissue Regeneration," *Molecules,* vol. 23, pp. 2651-2667, 2018.

[28] N. Hu, Z. Yang, Y. Wang, L. Zhang, Y. Wang, X. Huang, H. Wei, L. Wei and Y. Zhang, "Ultrafast and sensitive room temperature NH3 gas sensors based on chemically reduced graphene oxide," *Nanotechnology,* vol. 25, no. 2, pp. 25502-25510, 2013.

[29] C.-J. Shih, S. Lin, R. Sharma, M. S. Strano and D. Blankschtein, "Understanding the pH-dependent behavior of graphene oxide aqueous solutions: A comparative experimental and molecular dynamics simulation study," *Langmuir,* vol. 28, no. 1, pp. 235-241, 2012.

[30] L. Wu, L. Liu, B. Gao, R. Muñoz-Carpena, M. Zhang, H. Chen, Z. Zhou and H. Wang, "Aggregation kinetics of graphene oxides in aqueous solutions: Experiments, mechanisms, and modeling," *Langmuir,* vol. 29, no. 49, pp. 15174-15181, 2013.

[31] C. A. Schneider, W. S. Rasband and K. W. Eliceiri, "NIH Image to ImageJ: 25 years of image analysis," *Nature Methods,* vol. 9, pp. 671-675, 2012.

[32] L. Lai, G. Carman, S. Chiou, P. Kukuchek and D. Echternach, "Processing monitoring of carbon/phenolic omposites using smart sensors," *Smart Materials and Structures,* vol. 4, pp. 118-125, 1995.

[33] M. Sernek and F. A. Kamke, "Application of dielectric analysis for monitoring the cure process of phenol formaldehyde adhesive," *International Journal of Adhesion & Adhesives ,* vol. 27, p. 562–567, 2007.

[34] U. Müller, C. Pretschuh, E. Zikulnig-Rusch, E. Dolezel-Horwath, M. Reiner and S. Knappe, "Dielectric analysis as cure monitoring system for melamine-formaldehyde laminates," *Progress in Organic Coatings ,* vol. 90, p. 277–283, 2016.

[35] F. Ciucci, "Modeling electrochemical impedance spectroscopy," *Current Opininion in Electrochemistry,* vol. 13, pp. 132-139, 2019.

[36] E. Barsoukov and J. Macdonald, Impedance Spectroscopy: Theory, Experiment, and Applications, Hoboken,NJ: John Wiley & Sons, Inc, 2005.

[37] C. Zhang, W. Lv, X. Xie, D. Tang, C. Liu and Q.-H. Yang, "Towards low temperature thermal exfoliation of graphite oxide for graphene production," *Carbon,* vol. 62, pp. 11-24, 2013.

[38] S. Claramunt, A. Varea, D. Lopez-Diaz, M. M. Velazquez, A. Cornet and A. Cicera, "The Importance of Interbands on the Interpretation of the Raman Spectrum of Graphene Oxide," *The Journal of Physical Chemistry C,* vol. 119, pp. 10123-10129, 2015.

[39] S. Farah, A. Farkas, J. Madarász and K. László, "Comparison of thermally and chemically reduced graphene oxides by thermal analysis and Raman spectroscopy," *Journal of Thermal Analysis and Calorimetry,* vol. 142, p. 331–337, 2020.

[40] P. Chen, H. Li, H. Yi, F. Jia, L. Yang and S. Song, "Removal of graphene oxide from water by floc-flotation," *Separation and Purification Technology,* vol. 202, p. 27–33, 2018.

[41] K. Muthoosamy and S. Manickam, "State of the art and recent advances in the ultrasound-assisted synthesis, exfoliation and functionalization of graphene derivatives," *Ultrasonics - Sonochemistry ,* vol. 39, pp. 478-493, 2017.

[42] S. . M. Mahdi Alavi, A. Mahdi, S. J. Payne and D. A. Howey, "Identifiability of Generalized Randles Circuit Models," *IEEE TRANSACTIONS ON CONTROL SYSTEMS TECHNOLOGY,* vol. 25, no. 6, pp. 2112-2120, 2017.

[43] M. E. Orazem and B. Tribollet, Electrochemical Impedance Spectroscopy, Hoboke, NJ: Wiley, 2008.

[44] K. I. Han, S. D. Kim, W. S. Yang, H. S. Kim, M. Shin, J. P. Kim, I. G. Lee, B. J. Cho and W. S. Hwang, "Material characteristics and equivalent circuit models of stacked graphene oxide for capacitive humidity sensors," *AIP Advances,* vol. 6, p. 035203, 2016.

[45] M. W. Hahn and C. R. O'Melia, "Deposition and Reentrainment of Brownian Particles in Porous Media under Unfavorable Chemical Conditions: Some Concepts and Applications," *Environmental Science & Technology,* vol. 38, no. 1, pp. 210-220, 2004.

[46] H. Wang and Y. H. Hu, "Electrolyte-induced precipitation of graphene oxide in its aqueous solution," *Journal of Colloid and Interface Science,* vol. 391, pp. 21-27, 2013.

[47] P. Mirtaheri, S. Grimnes and G. Martinsen, "Electrode polarization impedance in weak NaCl aqueous solutions," *IEEE Transactions on Biomedical Engineering,* vol. 52, no. 12, pp. 2093-2099, 2005.

[48] G. R. Olhoeft, "Low-frequency electrical properties," *GEOPHYSICS,* vol. 20, no. 12, pp. 2492-2503, 1985.

675

676